Local and Global Effects of Metal Binding within the Small Subunit of Ribonucleotide Reductase

Brad S. Pierce and Michael P. Hendrich*

Contribution from the Department of Chemistry, Carnegie Mellon University, Pittsburgh, Pennsylvania 15213

Received February 13, 2004; Revised Manuscript Received October 21, 2004; E-mail: hendrich@andrew.cmu.edu

Abstract: Each β-protomer of the small $\beta\beta$ subunit of *Escherichia coli* ribonucleotide reductase (R2) contains a binuclear iron cluster with inequivalent binding sites: Fe_A and Fe_B. In anaerobic Fe^{II} titrations of apoprotein under standard buffer conditions, we show that the majority of the protein binds only one Fe^{II} atom per $\beta\beta$ subunit. Additional iron occupation can be achieved upon exposure to O_2 or in high glycerol buffers. The differential binding affinity of the A- and B-sites allows us to produce heterobinuclear $Mn^{II}Fe^{II}$ and novel $Mn^{III}Fe^{III}$ clusters within a single β-protomer of R2. The oxidized species are produced with H_2O_2 addition. We demonstrate that no significant exchange of metal occurs between the A- and B-sites, and thus the binding of the first metal is under kinetic control, as has been suggested previously. The binding of first Fe^{II} atom to the active site in a β-protomer (β_I) induces a *global* protein conformational change that inhibits access of metal to the active site in the other β-protomer (β_{II}). The binding of the same Fe^{II} atom also induces a *local* effect at the active site in β_I-protomer, which lowers the affinity for metal in the A-site. The mixed metal FeMn species are quantitatively characterized with electron paramagnetic resonance spectroscopy. The previously reported catalase activity of $Mn_2^{II}R2$ is shown not to be associated with Mn.

Introduction

Ribonucleotide reductase (RNR) catalyzes the reduction of nucleotide diphosphates (NDP) to deoxynucleotide diphosphates (dNDP) for DNA synthesis.[1] As isolated from *Escherichia coli*, RNR is composed of two homodimeric subunits ($\alpha_2\beta_2$). The α_2 subunit (R1) is the larger of the two homodimers and contains the substrate binding site and at least two allosteric effector sites. Each monomer of the R1 subunit contains five conserved redox-active cysteine residues essential for catalytic activity.[1-3] Three of these cysteines, located within the active site of R1, are directly involved in the reduction of NDPs.[4,5]

Each polypeptide chain within the smaller $\beta\beta$ subunit (R2) contains the binuclear non-heme iron site. This subunit belongs to a diverse group of proteins that are capable of reductively activating O_2 in order to perform a variety of biological reactions.[6] In the reduced state ($R2_{red}$), the diferrous site can reductively activate O_2 and, combined with an "extra" electron, produce a stable tyrosine radical (Y122•) adjacent to the diiron active site.[6-19] The Y122• on R2 is essential for the catalytic

activity of RNR and is believed to initiate a thiol radical (C439) within the active site of R1 through a long-range proton-coupled electron transport (PCET) pathway.[3,5] The structure of diferrous clusters in $R2_{red}$ is shown in Figure 1.[8,18,19]

Mössbauer and MCD studies have shown that the Fe_B site[20] (spectroscopically assigned to the Fe2, 8.3 Å from Y122) exhibits approximately a 5-fold greater binding affinity for Fe^{II} than the Fe_A site (spectroscopically assigned to the Fe1, 5.3 Å from Y122).[18,19,21-23] We have previously demonstrated that under standard buffer conditions, the two β-protomers of R2 do not act independently during metal incorporation. Under nonturnover conditions, only a single β-strand of R2 is capable

(1) Stubbe, J. *Adv. Enzymol. Relat. Areas Mol. Biol.* **1990**, *63*, 349–419.
(2) Reichard, P. *Trends Biochem. Sci.* **1997**, *22*, 81–85.
(3) Stubbe, J.; Nocera, D. G.; Yee, C. S.; Chang, M. C. Y. *Chem. Rev.* **2003**, *103*, 2167–2202.
(4) Stubbe, J. *J. Biol. Chem.* **1990**, *265*, 5329–5332.
(5) Ge, J.; Yu, G.; Ator, M. A.; Stubbe, J. *Biochemistry* **2003**, *42*, 10071–10083.
(6) Feig, A. L.; Lippard, S. J. *Chem. Rev.* **1994**, *94*, 759–805.
(7) Wallar, B. J.; Lipscomb, J. D. *Chem. Rev.* **1996**, *96*, 2625–2657.
(8) Nordlund, P.; Eklund, H. *J. Mol. Biol.* **1993**, *232*, 123–164.
(9) Bollinger, J. M., Jr.; Krebs, C.; Vicol, A.; Chen, S.; Ley, B. A.; Edmondson, D. E.; Huynh, B. H. *J. Am. Chem. Soc.* **1998**, *120*, 1094–1095.
(10) Nordlund, P.; Aaberg, A.; Uhlin, U.; Eklund, H. *Biochem. Soc. Trans.* **1993**, *21*, 735–738.
(11) Nordlund, P.; Sjoeberg, B. M.; Eklund, H. *Nature* **1990**, *345*, 593–598.
(12) Thelander, L. *J. Biol. Chem.* **1974**, *249*, 4858–4862.
(13) Reichard, P. *Science* **1993**, *260*, 1773–1777.
(14) Bollinger, J. M., Jr.; Edmondson, D. E.; Huynh, B. H.; Filley, J.; Norton, J. R.; Stubbe, J. *Science* **1991**, *253*, 292–298.
(15) Baldwin, J.; Krebs, C.; Ley, B. A.; Edmondson, D. E.; Huynh, B. H.; Bollinger, J. M., Jr. *J. Am. Chem. Soc.* **2000**, *122*, 12195–12206.
(16) Lynch, J. B.; Juarez-Garcia, C.; Munck, E.; Que, L., Jr. *J. Biol. Chem.* **1989**, *264*, 8091–8096.
(17) Atkin, C. L.; Thelander, L.; Reichard, P. *J. Biol. Chem.* **1973**, *248*, 7464–7472.
(18) Logan, D. T.; Su, X.-D.; Aaberg, A.; Regnstroem, K.; Hajdu, J.; Elkund, H.; Nordlund, P. *Structure* **1996**, *4*, 1053–1064.
(19) Andersson, M. E.; Hoegbom, M.; Rinaldo-Matthis, A.; Andersson, K. K.; Sjoeberg, B.-M.; Nordlund, P. *J. Am. Chem. Soc.* **1999**, *121*, 2346–2352.
(20) The use of FeA and FeB to designate the crystallographic iron sites Fe1 and Fe2 reported by Nordlund et al. was originally invoked by Ravi et al. to clarify comparisons made between the crystallographic work and their Mössbauer assignments. Subsequently, this nomenclature has been adopted by several other researchers spectroscopically characterizing the individual iron binding sites of R2.
(21) Yang, Y.-S.; Baldwin, J.; Ley, B. A.; Bollinger, J. M., Jr.; Solomon, E. I. *J. Am. Chem. Soc.* **2000**, *122*, 8495–8510.
(22) Bollinger, J. M., Jr.; Chen, S.; Parkin, S. E.; Mangravite, L. M.; Ley, B. A.; Edmondson, D. E.; Huynh, B. H. *J. Am. Chem. Soc.* **1997**, *119*, 5976–5977.
(23) Ravi, N.; Bollinger, J. M., Jr.; Huynh, B. H.; Stubbe, J.; Edmondson, D. E. *J. Am. Chem. Soc.* **1994**, *116*, 8007–8014.
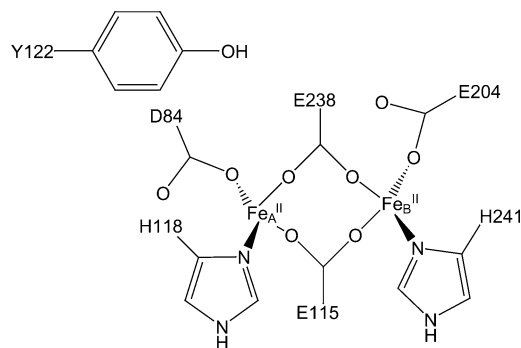
Figure 1. Schematic representation of the diferrous R2 active site adapted from references.[8,18,19]

of Mn^{II} incorporation. Subsequently, we have introduced nomenclature to differentiate the β-protomer which initially binds metal as β_I and the adjacent second β-protomer as β_{II}.[24] We also demonstrated that binding of metal into the β_{II} protomer occurs during or after activation of R2 with O_2.

Previous studies of the kinetics of the O_2 reaction with R2 have shown an order of magnitude rate increase for R2 preloaded with 2 equiv of Fe^{II} over apoR2.[23,25] On the basis of that work, it was proposed that the slow step in apoR2 is a protein conformation change that occurs during the preloading of iron.[26,27] An implicit assumption in this previous work was that the preloading step involved binding of Fe^{II} into the two Fe_B sites of the homodimer of R2. However, our previous work indicates that the β_{II} protomer is not occupied during such preloading and that a protein conformational change occurs upon loading of the first metal into the β_I protomer. Thus, in the absence of oxygen we can focus solely on the metal loading within a single β-protomer.

Protein-bound mononuclear ferrous iron is spectroscopically difficult to accurately differentiate from adventitious Fe^{II}, and thus our initial work used paramagnetic Mn^{II} ion as a spectroscopic probe for Fe^{II} binding within the apoR2 homodimer. Here we focus on the effects due to iron and present four new results with respect to metal binding. (1) We now show direct quantitative spectroscopic results for Fe^{II}-only titrations, indicating that Fe^{II} bound within the B-site significantly decreases the affinity for Fe^{II} (the native metal) within the adjacent A-site. For higher concentrations of added Fe^{II}, a small amount of diferrous clusters is formed, but these clusters are not the majority Fe^{II} species. (2) We show that Fe^{II} bound within the B-site also significantly decreases the affinity for Mn^{II} within the adjacent A-site. (3) As previously observed for Mn additions, Fe^{II} binding in the B-site of a single protomer shows a negative allosteric effect on metal incorporation within the opposite β-protomer. (4) In the reverse addition, Mn^{II} or Fe^{II} added to samples of apoR2 preloaded with a single equivalent of Mn^{II} generates the $Mn_A^{II}Mn_B^{II}$ or $Fe_A^{II}Mn_B^{II}$ cluster, respectively, within a single β-strand of R2.

The results indicate that the occupation of one B-site with ferrous iron affects both *local* and *global* occupation of the other three metal binding sites. The results are consistent with our

previous conclusion of a protein conformation change upon loading of a single equivalent of metal into the homodimer R2. We suggest that the *global* effect is a protein conformational change that affects access to the active site, whereas the *local* effect is a change in the active site that affects the binding constant of the second metal.

New electron paramagnetic resonance (EPR) signals are presented here for three different states of the mixed metal protein: $Fe_A^{II}Mn_B^{II}$, $Fe_A^{III}Mn_B^{III}$, and $Mn_A^{III}Fe_B^{III}$. These signals are assigned, and the electronic properties of the respective clusters are characterized. The $Fe^{III}Mn^{III}$ R2 dinuclear sites are produced by anaerobic sequential addition of Fe^{II} and Mn^{II} to R2 followed by addition of H_2O_2. We have prepared isolated samples of each oxidized mixed metal species. The hyperfine contributions of the Mn^{III} ion determine a unique ground-state electronic configuration for each site.

The reaction of O_2 with $Mn^{II}Fe^{II}$ R2 sites does not produce $Mn^{III}Fe^{III}$ R2 sites. However, we observed the formation of a minority amount of $Mn^{III}Fe^{III}$ R2 sites during multiple turnover reactions of the protein in the presence of dithionite, mediator, and O_2. During these reactions, the only oxidants present are O_2 and the high oxidation states of the diiron cluster (e.g., intermediate X). Since the reaction of O_2 with $Mn^{II}Fe^{II}$ R2 sites does not produce the $Mn^{III}Fe^{III}$ R2 sites, one dinuclear site must serve as an electron source for another site in the generation of the active form of R2 [$Fe_2^{III}R2$; Tyr•], $R2_{act}$. Therefore, in part, the substoichiometric yield of Y122• per R2 could be a result of inter- and/or intraprotein electron transfer between the active sites of R2.

Previous publications have reported catalase activity from Mn-incorporated R2 samples.[28,29] We show here that such activity is not associated with Mn incorporation.

Materials and Methods

Protein Purification. R2 was isolated from an overproducing strain of *E. coli* N6405/pSPS2 as previously described.[30−32] During purification, proteolytic degradation of R2 was decreased by addition of a general purpose cocktail of protease inhibitors (Sigma P 2714). After iron chelation, the buffer was exchanged by passing the protein solution down a Sephadex G-25 size exclusion column [1.9 × 38 cm] equilibrated with 25 mM 4-(2-hydroxyethyl)piperazine-1-ethanesulfonic acid (HEPES), 100 mM KCl, and 5% glycerol, pH 7.6. Significant amounts of denatured R2 were produced during chelation. After the column, the denatured protein was pelleted with centrifugation. UV/vis measurements were made on a HP 8453 spectrophotometer equipped with a constant temperature cuvette holder. The protein concentration was determined spectrophotometrically from the absorbance at 280 nm [ϵ_{280} = 141 mM^{-1} cm^{-1} (R2) and 126 mM^{-1} cm^{-1} (apoR2)].[32]

Sample Preparation. Stock Mn^{II} and Fe^{II} solutions were prepared anaerobically by dissolving $MnCl_2$ or $Fe(NH_3)_2(SO_4)_2$ within degassed protein buffer or double distilled water, respectively. The concentration of the Mn^{II} stock solution was determined from quantification of the EPR signal. The Fe^{II} stock solutions were assayed spectrophotometrically as described previously.[24] These stock solutions (typically 10−20 mM in metal) were prepared fresh prior to addition to apoR2. For each metal addition, the appropriate amount of metal containing stock

(24) Pierce, B. S.; Elgren, T. E.; Hendrich, M. P. *J. Am. Chem. Soc.* **2003**, *125*, 8748−8759.
(25) Bollinger, J. M., Jr.; Tong, W. H.; Ravi, N.; Huynh, B. H.; Edmonson, D. E.; Stubbe, J. *J. Am. Chem. Soc.* **1994**, *116*, 8015−8023.
(26) Tong, W. H.; Chen, S.; Lloyd, S. G.; Edmonson, D. E.; Huynh, B. H.; Stubbe, J. *J. Am. Chem. Soc.* **1996**, *118*, 2107−2108.
(27) Umback, N. J.; Norton, J. R. *Biochemistry* **2002**, *41*, 3984−3990.

(28) Hogbom, M.; Andersson, M. E.; Nordlund, P. *J. Biol. Inorg. Chem.* **2001**, *6*, 315−323.
(29) Elgren, T. E.; Marcoline, A. T.; Goldstein, J. I. *J. Inorg. Biochem.* **1999**, *74*, 122.
(30) Bollinger, J. M., Jr.; Tong, W. H.; Ravi, N.; Huynh, B. H.; Edmondson, D. E.; Stubbe, J. *J. Am. Chem. Soc.* **1994**, *116*, 8024−8032.
(31) Salowe, S. P.; Stubbe, J. *J. Bacteriol.* **1986**, *165*, 363−366.
(32) Lynch, J. B. Ph.D. Thesis, University of Minnesota, 1989.

solution (typically 5−10 μL) was added anaerobically to solution of apoR2 (initially 150−200 μL of 1 mM R2) directly within the EPR tube with a 25 μL Hamilton gastight syringe. The solution was mixed with a second gastight syringe (250 μL) and by inversion for 5 min, and then the sample was frozen in liquid N_2. H_2O_2 solutions were prepared by dilution of a 30% stock solution in buffer. Determination of H_2O_2 concentration was performed spectrophotometrically from the absorbance at 230 nm [ϵ_{230} = 72.8 M^{-1} cm^{-1}].[33] The resulting solution was degassed prior to use.

Catalase Activity. Dioxygen content was assayed polarographically using a standard Clark electrode within a 1.5-mL water-jacketed cell. Experiments were run at 25 ± 2 °C and controlled by a circulating water bath. The oxygen electrode was calibrated from the voltage difference after addition of a known amount of H_2O_2 (confirmed spectrophotometrically) to a solution containing bovine liver catalase (Sigma C-9322). From the voltage difference an electrode constant could be determined.

Metal Analysis. Samples of apoR2 were analyzed for metal content by inductively coupled plasma emission spectroscopy (ICP ES) at the University of Minnesota, Research Analytical Laboratory, Department of Soil, Water, and Climate. ICP samples were prepared by digesting protein in ultrapure concentrated HCl (0.5 mL of HCl diluted to 5 mL with double distilled H_2O) followed by boiling for 30 minutes. The resulting suspension was centrifuged to pellet undigested protein. Supernatant was taken for analysis. To determine that nearly all metal was extracted from the protein, a second sample was prepared from the pellet following the same technique described above.

Chemicals. All chemicals were purchased from Sigma, Fisher, or VWR and used without purification. The water was from a Millipore-Q filtration system or double distilled. All aqueous solutions prepared for protein work were made within a 25 mM HEPES, 100 mM KCl, 5% glycerol, pH 7.6 buffer except where noted.

EPR Spectroscopy. X-band (9 GHz) EPR spectra were recorded on a Bruker ESP 300 spectrometer equipped with an Oxford ESR 910 cryostat for low-temperature measurements and a Bruker bimodal cavity for generation of the microwave fields parallel and transverse to the static field. The microwave frequency was calibrated by a frequency counter, and the magnetic field was calibrated with a NMR gaussmeter. The temperature was calibrated with resistors (CGR-1−1000) from Lake Shore Cryonics. A modulation frequency of 100 kHz was used for all EPR spectra. All experimental data were collected under nonsaturating conditions.

EPR Simulations. Analysis of the EPR spectra utilized the spin Hamiltonian:

$$H_S = -2J(S_1 \cdot S_2) + \sum_{i=1,2} S_i \cdot \mathbf{D} \cdot S_i + \beta(S_i \cdot \mathbf{g}_i \cdot B) + S_i \mathbf{A}_i I_i \quad (1)$$

where **D** describes the axial zero-field splitting (zfs) parameter and **g** is the g-tensor.[34] Nuclear hyperfine interactions (**A**) are treated with second-order perturbation theory. In the case of $J/D \gg 1$, the above spin Hamiltonian simplifies to the following:

$$H_s = \beta(S_C \cdot \mathbf{g}_i \cdot B) + S_C \cdot \mathbf{A} \cdot I \quad (2)$$

where S_C is the coupled spin state. Simulations of the EPR spectra are calculated from diagonalization of this equation with software created by the authors. The simulations are generated with consideration of all intensity factors both theoretical and experimental to allow concentration determination of species.[35] This allows direct comparison of simulated spectra to the absolute intensity scale of the experimental spectrum
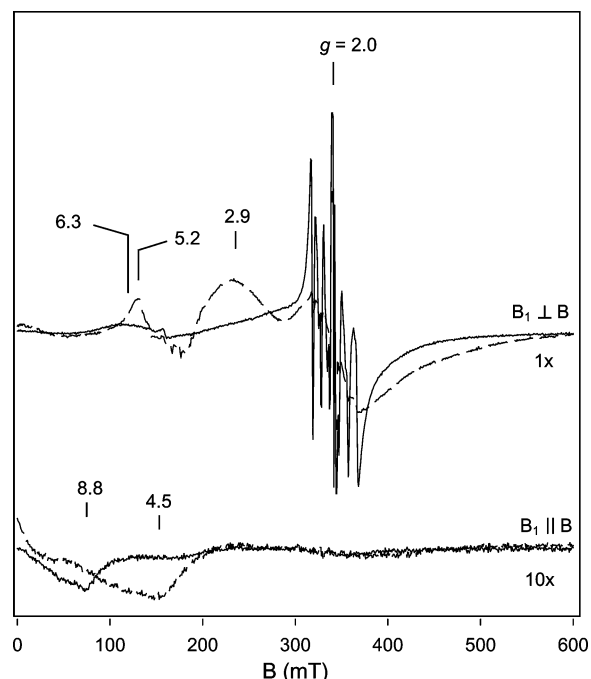
(33) Foote, C. S.; Valentine, J. S.; Greenberg, A.; Liebman, J. F. *Active Oxygen In Chemistry*; Chapman & Hall: New York, 1995; Vol. 2.
(34) Abragam, A.; Bleaney, B. *Electron Paramagnetic Resonance of Transition Ions*; Clarendon Press: Oxford, 1970.
(35) Hendrich, M. P.; Petasis, D.; Arciero, D. M.; Hooper, A. B. *J. Am. Chem. Soc.* **2001**, *123*, 2997−3005.
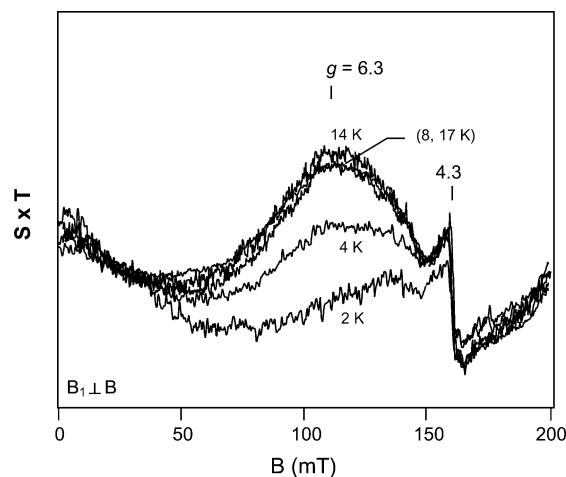
Figure 2. Perpendicular- (⊥) and parallel-mode (||) EPR spectra of Mn_B^{II}-R2 before (dashed lines) and after addition of Fe^{II} (solid lines). The parallel-mode signal intensity was scaled by 10×. Sample conditions: 1.23 mM apoR2, 0.63 mM Mn^{II}, 3.1 mM Fe^{II}, 25 mM HEPES, 100 mM KCl, 5% glycerol, pH 7.6. Instrumental conditions: temperature, 9 K; microwave power, 0.02 mW (⊥), 0.2 mW (||); microwave frequency, 9.62 GHz (⊥), 9.27 GHz (||).

having a known sample concentration. The only unknown factor relating the spin concentration to signal intensity is an instrumental factor that depends on the microwave detection system. However, this factor is determined by the spin standard, CuEDTA, for which the copper concentration was accurately determined from plasma emission spectroscopy.

Results

Formation of the ($Fe_A^{II}Mn_B^{II}\beta_I$) Cluster, Sample 1a. To a sample of apoR2, 0.5 equiv of Mn^{II} was added to the protein under strict anaerobic conditions via a Hamilton gastight syringe and allowed to equilibrate for 5 min prior to freezing. Figure 2 shows X-band EPR spectra of this sample for microwave fields perpendicular ($B_1 \perp B$) and parallel ($B_1 || B$) to the static magnetic field at 9 K before (dashed lines) and after (solid lines) addition of Fe^{II}. The broad signals (dashed lines) observed at g = 5.2, 2.9, and 2.0 ($B_1 \perp B$) and g = 4.5 ($B_1 || B$) originate from mononuclear bound Mn^{II} within the active site of R2. Given the greater binding affinity observed for the B-site,[21,22] this signal was assigned to Mn^{II} bound within the B-site of R2 (Mn_B^{II}R2) and quantified as 0.5 equiv as previously characterized.[24] The sharp six-line hyperfine pattern observed at g = 2.0 is attributed to adventitious hexaqua ligated Mn^{II}, termed aquaMn^{II}, and accounts for <2% of the total Mn^{II} added. The signal intensity of both species is observed to be inversely proportional to temperature.

Upon addition of 5 equiv of Fe^{II} (solid lines), all EPR signals attributed to Mn_B^{II}R2 disappear, the aquaMn^{II} signal intensity increases, and two new signals are observed at g = 8.8 ($B_1 || B$) and g = 6.3 ($B_1 \perp B$) from two different species. The signal at g = 8.8 ($B_1 || B$) is characteristic of aquaFe^{II} and will be discussed in more detail below. The increased amount of

Figure 3. Perpendicular-mode EPR spectra of **1a** at temperatures $T = 2$, 4, 8, 14, and 17 K. Each spectra was plotted as signal × T. The $g = 4.3$ signal is from trace (<5 μM) ferric iron contamination. Sample conditions same as those in Figure 2.

aquaMn^{II} displaced upon 5× addition of Fe^{II} corresponds to 20% of the total Mn^{II} added. However, stoichiometric addition of Fe^{II} with Mn^{II} also results in the loss of Mn^{II}R2 signals, with less than 5% of the total Mn^{II} displaced (data not shown). The loss of the Mn^{II}R2 signal indicates that Fe^{II} must bind adjacent to the Mn$_B$ site to give an exchange-coupled Fe^{II}Mn^{II} cluster.

An antiferromagnetically coupled Fe^{II} ($S = 2$) Mn^{II} ($S = 5/2$) cluster with $J/D_{Fe} \gg 1$ should show an EPR signal from the ground $S_C = 1/2$ doublet near $g = 2$. No evidence for such a signal is observed, but small amounts of aquaMn^{II} also produce signals in this region that can easily obliterate the $S_C = 1/2$ signal. Alternatively, for a species with only carboxylates bridging the metals, we expect a weak exchange interaction $|J| < 2$ cm^{-1} ($H = -2JS_1 \cdot S_2$). Typical values of $|D_{Fe}|$ for Fe^{II} range from 3 to 11 cm^{-1}, thus $J/D_{Fe} \leq 1$.[36-38] For this case, the coupled system spin states are not good quantum numbers and the spectra are more complicated. As shown in Figure 3, the $g = 6.3$ (**B$_1$ $\perp$ B**) signal is observed to grow in at higher temperatures and is nearly absent at low temperature, indicating that this signal originates from an excited doublet. We attribute the $g = 6.3$ (**B$_1$ $\perp$ B**) signal to a weakly coupled Fe$_A^{II}$Mn$_B^{II}$ cluster as demonstrated next.[39]

Scheme 1 illustrates the relative placement of the first six doublets for a weakly coupled $J/D_{Fe} < 1$ Fe^{II}Mn^{II} cluster. Figure 4 shows the X-band EPR spectrum of **1a** at 9 K overlaid on a simulation for a weakly coupled system, $S_{Fe} = 2$ and $S_{Mn} = 5/2$, $I_{Mn} = 5/2$. The spectra was fit reasonably well with $|D_{Fe}| = 9$ cm^{-1}, $E_{Fe}/D_{Fe} = 0.33$, and $|D_{Mn}| = 0.1$ cm^{-1}, $E_{Mn}/D_{Mn} = 0.21$, $A_{Mn} = 250$ MHz, and $J = -1.3$ cm^{-1}. Furthermore, as mentioned in the Materials and Methods section, the simulation method links the signal intensity to the sample concentration. The amount of **1a** predicted from simulation is within 13% of unaccounted [Mn^{II}] after addition of Fe^{II}. Therefore, within experimental error, all of the metal added to apoR2 is accounted
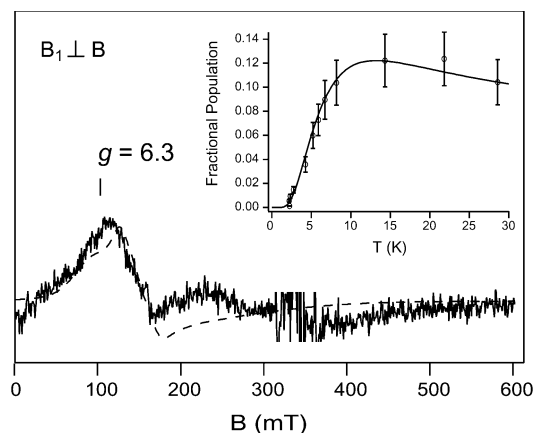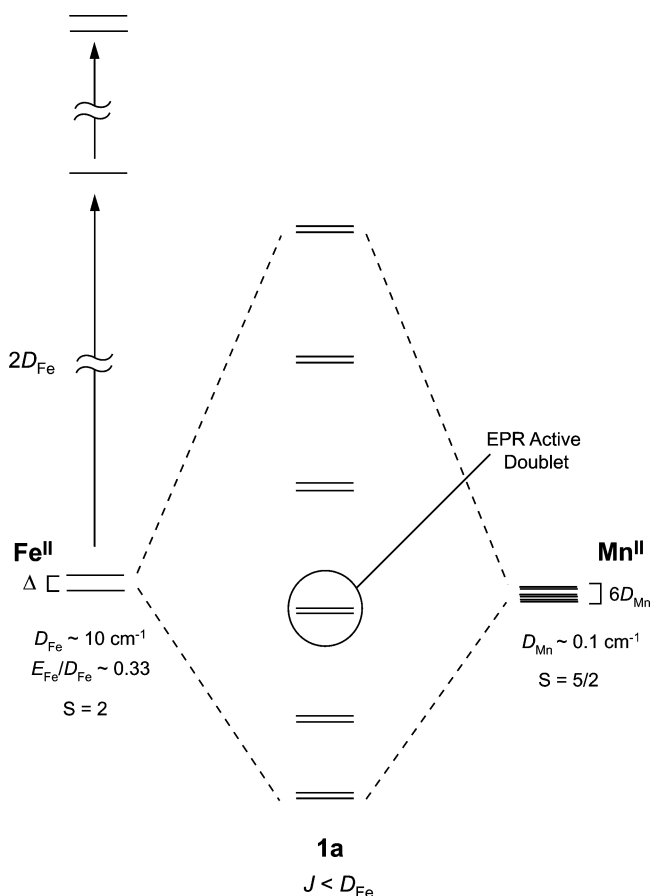
(36) Hendrich, M. P.; Debrunner, P. G. *Biophys. J.* **1989**, *56*, 489−506.
(37) Clay, M. D.; Jenney, F. E., Jr.; Hagedoorn, P. L.; George, G. N.; Adams, M. W. W.; Johnson, M. K. *J. Am. Chem. Soc.* **2002**, *124*, 788−805.
(38) Knapp, M. J.; Krzystek, J.; Brunel, L. C.; Hendrickson, D. N. *Inorg. Chem.* **2000**, *39*, 281−288.
(39) Near the axial limit (E/D $\approx$ 0), the theoretical signal intensity for doublets that could possibly give the desired temperature profile is too weak to explain the observed signal. However, near the rhombic limit (E/D $\approx$ 1/3), the transition probabilities increase significantly.

Figure 4. Perpendicular-mode EPR spectra of **1a** (solid line) and simulation (broken line) at 9 K. Inset: Intensity of the $g = 6.3$ (B$_1$ $\perp$ B) signal × temperature versus temperature. The theoretical curve is the fractional population of the second excited doublet illustrated in Scheme 1 for $J = -1.3 \pm 0.4$ cm^{-1}. The aquaMn^{II} signal at $g = 2$ was subtracted out for clarity. Instrumental conditions: microwave power, 0.02 mW; microwave frequency, 9.62 GHz. Simulation parameters: $S_{Fe} = 2$, $|D_{Fe}| = 8.8$ cm^{-1}, $\sigma_D = 2.9$ cm^{-1}, $E_{Fe}/D_{Fe} = 0.33$, $\sigma_{E/D} = 0.10$, $S_{Mn} = 5/2$, $I_{Mn} = 5/2$, $A_{Mn} = 250$ MHz, $D_{Mn} = 0.10$ cm^{-1}, $\sigma_D = 0.03$ cm^{-1}, $E_{Mn}/D_{Mn} = 0.21$, $\sigma_{E/D} = 0.05$, $J = 1.3$ cm^{-1}, $\sigma_B = 1.0$ mT .

Scheme 1

for. The EPR signal originates from the second excited doublet of Scheme 1. The high rhombicity of the Fe^{II} site is reasonable given the low symmetry of the crystal structure. The Mn^{II} parameters of the simulation are taken from those of the mononuclear site. However, significant changes in these values have little effect on the simulation. Unresolved hyperfine from manganese and distributions in D and E/D are found to dominate
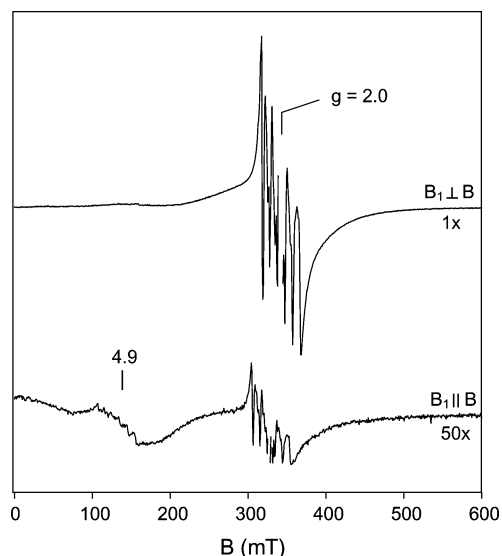
Figure 5. Perpendicular- ($\perp$) and parallel-mode ($||$) EPR spectra of Fe_B^{II}-R2 after stoichiometric addition of Mn^{II}. The signal at $g = 2.0$ from trace $Y_{122}\bullet$ ($\sim$0.06 mM) was deleted for clarity. The parallel-mode signal intensity was scaled by $50\times$ for comparison. Sample conditions: 0.80 mM apoR2, 0.80 mM Mn^{II}, 0.80 mM Fe^{II}, 25 mM HEPES, 100 mM KCl, 5% glycerol, pH 7.6. Instrumental conditions: temperature, 2.3 K; microwave power, 2.0 μW ($\perp$), 0.2 mW ($||$); microwave frequency, 9.62 GHz ($\perp$), 9.27 GHz ($||$).

the line width of the signal. The observed line width is fit for Gaussian distributions of $\sigma_D = 2.9$ and 0.03 cm^{-1}, and $\sigma_{E/D} = 0.10$ and 0.05 for Fe^{II} and Mn^{II}, respectively.

The inset of Figure 4 illustrates the temperature dependence of the $g = 6.3$ ($B_1 \perp B$) signal intensity times temperature versus temperature. The theoretical curve is generated for a fractional Boltzmann population of the second excited doublet of **1a**. The temperature dependence of the signal intensity does not significantly depend on D_{Fe} within the range $3 < D_{Fe} < 11$ cm^{-1}. Thus, the value of $J = -1.3 \pm 0.4$ cm^{-1} can be determined from a fit to the data.

Addition of Mn^{II} to $Fe_B^{II}R2$, Sample 1b. We attempted to generate the complementary reduced mixed metal cluster (Mn_A^{II}-$Fe_B^{II}\beta_I$) in which the Mn and Fe occupation is reversed. One equivalent of Fe^{II} was added to a sample of apoR2 under strict anaerobic conditions and allowed to equilibrate for 5 min prior to freezing. The EPR spectrum of this sample (data not shown) shows a weak signal in parallel mode with a pronounced valley at $g = 8.8$ ($B_1 || B$). This signal, which will be discussed later, is indicative of high-spin ferrous iron and quantifies to 1.1 equiv of Fe^{II}.[37] An insignificant amount of Fe^{III} was observed at $g = 4.3$ ($B_1 \perp B$). Upon addition of 1 equiv of Mn^{II} to this sample, no protein-bound Mn^{II} species were observed. As shown in Figure 5, only the characteristic six-line signal at $g = 2.0$ ($B_1 \perp B$) of aquaMn^{II} is observed. The parallel-mode EPR signal observed at $g = 4.9$ ($B_1 || B$) exhibits a six-line pattern split by 9.4 mT. This signal is typical of aquaMn^{II} and originates from the $\Delta m_s = 2$ "half-field" transitions.[24] Double integration of the $g = 2.0$ signal ($B_1 \perp B$) accounts for essentially all (93%) of the total Mn^{II} added. Thus, apoR2 preloaded with a single equivalent of Fe^{II} does not bind a significant amount of Mn^{II} in either the adjacent A-site of β_I or within the vacant β-strand (β_{II}) of R2.

Fe^{II} Titration of apoR2. As shown above, addition of 1 equiv of Fe^{II} to apoR2 prevents Mn^{II} from binding either β-strand of
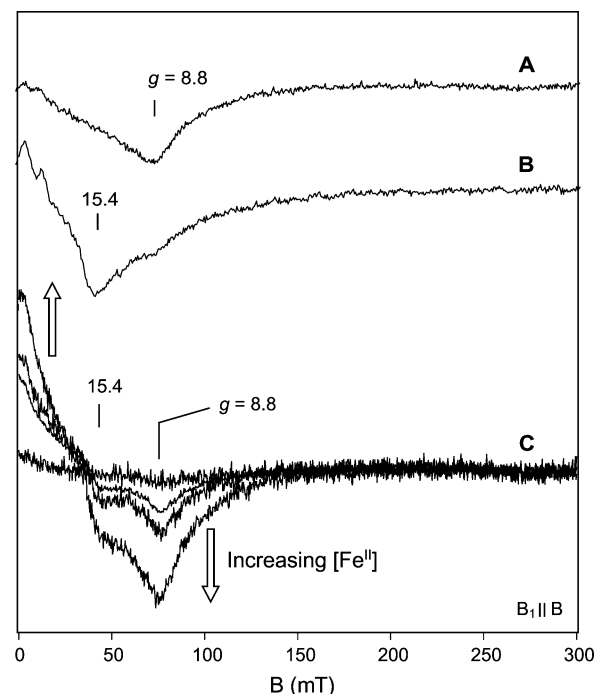

Figure 6. Parallel-mode EPR spectra of (A) aqueous ferrous iron, (B) the reduced diiron active site of R2 (R2$_{red}$), and (C) the anaerobic titration of apoR2 with ferrous iron. The arrows point in the direction of increasing [Fe^{II}] for the spectra in C. Sample conditions: (A) 10 mM $Fe(NH_4)_2(SO_4)_2$, (B) 0.76 mM R2$_{red}$, (C) 1 mM apoR2. All samples were prepared in 25 mM HEPES, 100 mM KCl, 5% glycerol, pH 7.6 buffer. The equivalents of added Fe^{II} per R2 are 1.2, 1.7, 2.9, and 5.6. Instrumental conditions: temperature, (A) 11 K, (B) 2 K, (C) 2 K; microwave power, (A) 2.0 mW, (B and C) 0.2 mW; microwave frequency, 9.27 GHz; $n = 15$ scans for (B).

R2. Thus, Fe^{II} binding within the B-site of apoR2 induces the same negative allosteric effect observed for Mn^{II},[24] resulting in the restriction of metal access within β_{II}. We refer to the negative allosteric affect on β_{II} caused by metal binding within β_I as the *global* conformational change. However, unlike Mn^{II}, ferrous iron also exhibits a *local* change that decreases the affinity of Mn^{II} within the adjacent A-site on β_I. To determine if this *local* change also affects the incorporation of the native ferrous metal, samples of apoR2 were titrated with Fe^{II} and the amount of mononuclear Fe^{II} and $Fe_2^{II}R2$ was followed by parallel-mode EPR spectroscopy.

To determine the concentration of each species, we compared the observed signals to samples of known concentration. Figure 6A shows an X-band parallel-mode EPR spectra of an aqueous Fe^{II} (10 mM) solution prepared anaerobically in buffer. This signal exhibits a pronounced valley at $g = 8.8$ ($B_1 || B$), which is linearly dependent on Fe^{II} concentration. We observe that this signal is not significantly affected by solvent conditions and introduction of nonmetal binding proteins. Therefore, the concentration of mononuclear Fe^{II} [mono-Fe^{II}] present in protein solutions can be determined from comparison to this aqueous Fe^{II} standard. The uncertainty in the determination of [mono-Fe^{II}] with this protocol is 20%.

HoloR2 can be prepared by addition of excess Fe^{II} and ascorbic acid to apoR2 under aerobic conditions,[17] followed by gel filtration to remove adventitious metal. For samples prepared in this manner, typically we observe 3.5 Fe and 1.2 tyrosine radicals per R2, which is consistent with published re-

Table 1. Mn^{III} Parameters for the Mixed Metal Fe^{III}Mn^{III}R2 Species

I. System and Intrinsic Mn^{III} Parameters

species	system A_1, A_2, A_3 MHz	intrinsic Mn^{III} A_1, A_2, A_3 MHz[c]	system g_1, g_2, g_3	intrinsic Mn^{III} g_1, g_2, g_3	reference
2a (Mn$_B$)	188, 310, 317	(−)141, (−)233, (−)238	2.044, 2.009, 2.033	1.967, 1.993, 1.975	this work
2b (Mn$_A$)	253, 370, 270	(−)190, (−)278, (−)203	2.041, 2.021, 2.015	1.969, 1.984, 1.989	this work
A[a]	222, 210, 236	(−)207, (−)207, (−)124	1.958, 1.965, 2.025	2.032, 2.023, 1.981	47
B[b]	314	235	2.037	1.950	45

II. Isotropic and Dipolar Contributions to the Mn^{III} Hyperfine Tensor

species	isotropic hyperfine (A_{iso})	dipolar hyperfine (A_{dip})	empty Mn^{III} d-orbital
2a (Mn$_B$)	−204 MHz	+31.5 MHz	($d_{x^2-y^2}$)
2b (Mn$_A$)	−223 MHz	−27.2 MHz	(d_{z^2})
A[a]	−179 MHz	+27.6 MHz	($d_{x^2-y^2}$)

[a] The intrinsic g-values for Mn^{III} were calculated assuming an isotropic Mn^{II} g-value of 2.0. **A** = Mn^{II}Mn^{III} state of manganese catalase from *Thermus Thermophilus*. [b] Only the isotropic value for each spectroscopic parameter was reported. **B** = Fe^{III}Mn^{III}(μ-O)(μ-MeCO$_2$)$_2$. [c] The signs given in parentheses are not obtained from simulation of the EPR spectra.

sults.[12,16,17,24,40] Upon reduction of this sample with sodium dithionite and methyl viologen (R2$_{red}$), the resulting EPR spectra (Figure 6B) exhibits a temperature-dependent EPR signal at g = 15.4 (**B$_1$** || **B**), which has been assigned to a ferromagnetically coupled Fe$_2^{II}$R2 cluster.[41] Samples prepared in this fashion represent the end result of metal loading and turnover with O$_2$; thus, after reduction, the active sites of both β-protomers contain ferrous iron. Furthermore, since no mono-Fe^{II} was observed by EPR upon reduction, all of the iron present in the sample must be contained within diferrous clusters. We will use this signal, which represents 1.75 Fe$_2^{II}$ clusters per R2 homodimer, to determine the concentration of diiron sites formed in the titration.

Figure 6C shows EPR spectra of four samples of apoR2 with increasing additions of Fe^{II}. Two spectroscopically distinct species are observed to grow with Fe^{II} addition. One species is observed at g = 8.8 (**B$_1$** || **B**), which is characteristic of a mononuclear Fe^{II} species. We cannot distinguish on the basis of the spectra if this species is hexaqua Fe, adventitious Fe, or an internal Fe binding site of R2, and thus we refer to this signal as the mono-Fe^{II} signal. The second species is observed at g = 15.4 (**B$_1$** || **B**) and has the same g-value, line shape, and temperature dependence as that of Fe$_2^{II}$R2 cluster of R2$_{red}$ described in the previous paragraph. For all of the titration samples, the amount of tyrosine radical observed by EPR was <6% of the total protein content, indicating that only a minor fraction of Fe was oxidized because of O$_2$ turnover chemistry of R2.

A comparison of signal intensities between the Fe-titrated apoR2 samples (Figure 6C) and the known aqueous Fe^{II} (Figure 6A) and holoR2 (Figure 6B) samples allows determination of the species concentration. Table 2 shows the species concentrations for mono-Fe^{II} and Fe$_2^{II}$R2 determined for each titration point. The sum of the EPR-determined mono-Fe^{II} and Fe$_2^{II}$R2 concentrations was found to equal the amount of Fe^{II} added to the sample. Thus, although we cannot differentiate between the different types of mononuclear Fe^{II} species, all of the Fe^{II} is quantitatively accounted for as either a mononuclear or dinuclear species. It is apparent from Table 2 that, upon titration of Fe^{II}, significantly less than one diferrous active site is produced per R2 homodimer. Of nearly 6 equiv of added Fe^{II}, only 0.6 equiv of Fe$_2^{II}$R2 is observed. If both β-protomers were capable of

(40) Bollinger, J. M., Jr.; Stubbe, J.; Huynh, B. H.; Edmondson, D. E. *J. Am. Chem. Soc.* **1991**, *113*, 6289−6291.
(41) Elgren, T. E.; Hendrich, M. P.; Que, L., Jr. *J. Am. Chem. Soc.* **1993**, *115*, 9291−9292.

Table 2. Distribution of Fe^{II} within the R2 Homodimer upon Titration of apoR2

[Fe]/[R2] [a]	[mono-Fe^{II}]/[R2]	[Fe$_2^{II}$R2]/[R2]	% mass balance[b]
0.3	0.3 ± 0.05	n/o[c]	96
1.7	1.3 ± 0.3	0.2 ± 0.1	100
2.9	2.0 ± 0.5	0.5 ± 0.1	99
5.6	3.7 ± 0.8	0.6 ± 0.1	89

[a] Each sample contained approximately 150 μL of 0.95 mM apoR2 prior to ferrous iron addition. [b] Percent mass balance is defined as the amount of Fe^{II} from each species divided by the amount of Fe^{II} added. [c] n/o: not observed.

binding metal, up to 2 equiv of Fe$_2^{II}$R2 sites should be produced. These data are a direct indication that dinuclear Fe^{II} clusters in R2 are not the predominate species formed in titration of Fe^{II}. Thus, the affinity of Fe^{II} for the A-site in the presence of Fe^{II} bound in the B-site is significantly lowered, and our observations extend to the biologically relevant metal. This is consistent with our previously published model of O$_2$-dependent metal incorporation of R2.

Formation of the Oxidized (Fe$_A^{III}$Mn$_B^{III}$$\beta_I$) and (Mn$_A^{III}Fe_B^{III}$-$\beta_I$) Clusters. Previously, we described an EPR signal that could only be simulated by a mixture of two spectroscopically distinct Mn^{III}Fe^{III} clusters (species **I** and **II**).[24] We speculated that these species were formed by the displacement of Fe^{II} by Mn^{II} within either the A- or B-site of R2 upon cycling the enzyme in the presence of dithionite, methyl viologen, and O$_2$. To confirm our assignments, samples of each oxidized mixed metal cluster (Mn$_A^{III}$Fe$_B^{III}$ and Fe$_A^{III}$Mn$_B^{III}$) were produced by addition of excess H$_2$O$_2$ (20 equiv) to samples **1a** and **1b** described above under anaerobic conditions. These samples were allowed to react for 15−20 min prior to quenching in liquid N$_2$. Figure 7 shows the EPR spectra after addition of H$_2$O$_2$ to each sample. For clarity, the signal from trace Y122● (<0.07 equiv) was cut from each spectrum. The addition of H$_2$O$_2$ to **1a** generates a new six-line signal near g = 2 with a hyperfine splitting of 11 mT (Figure 7A). A simulation of this species for a system spin of S = 1/2 is overlaid (dashed line) on the data of Figure 7A, and the parameters are given in Table 1. These parameters are more accurate than our previous values determined in the presence of two species, but they are essentially the same, confirming our previous assignment of this species to (Fe$_A^{III}$Mn$_B^{III}$)(β_{II}). We will refer to this species as **2a** henceforth. Quantitation of **2a** indicates that 0.5 equiv of the available **1a** was oxidized to produce (Fe$_A^{III}$Mn$_B^{III}$$\beta_I$)($\beta_{II}$). The Mn contained within **2a** and
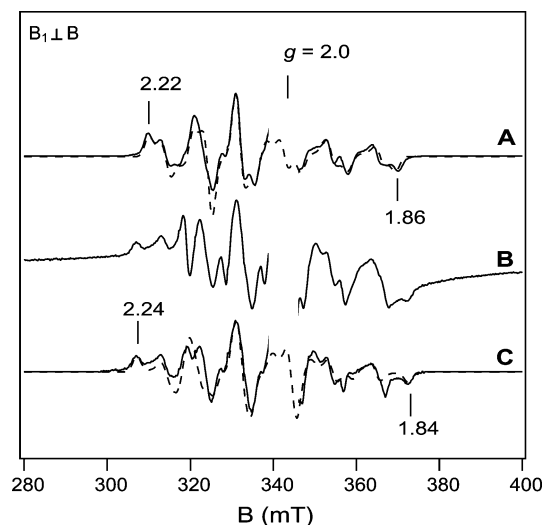
Figure 7. Perpendicular-mode EPR spectra for **1a** (A) and **1b** (B) after addition of H_2O_2. (C) Spectra of **2b** after subtraction of 0.4 equiv of aquaMn^{II} signal. The signal at $g = 2.0$ from trace $Y_{122}\bullet$ was deleted for clarity. Instrumental conditions: temperature, 11 K; microwave power, 0.2 μW; microwave frequency, 9.62 GHz. Simulation parameters for species **2a** and **2b** are given in Table 1.

an additional Mn$_2^{II}$R2 species (data not shown) account for the total Mn added to the sample.

The EPR spectrum of **1b** after H_2O_2 addition is shown in B. In this sample, two paramagnetic species are observed: an $S = 1/2$ signal and a $S = 5/2$ signal from aquaMn^{II}. Figure 7C shows the $S = 1/2$ signal after subtraction of the aquaMn^{II} signal. A simulation of this species for a system spin of $S = 1/2$ is overlaid (dashed line) on the data of Figure 7C, and the parameters are given in Table 1. The parameters are essentially the same as previously determined,[24] confirming our assignment of this species to (Mn$_A^{III}$Fe$_B^{III}$)(β_{II}), which we now refer to as species **2b**. Quantitation of **2b** and aquaMn^{II} accounts for 0.50 and 0.40 equiv of Mn, respectively. Therefore, upon addition of excess H_2O_2, **2b** is produced stoichiometrically with the loss of aquaMn^{II}.

Catalase Activity of Mn$_2^{II}$R2. Oxygen evolution from H_2O_2 addition to Mn-substituted R2 has been previously reported and attributed to catalase activity at the Mn$_2$ sites.[28,29] However, we do not observe an increase in the catalase activity of apoR2 upon incorporation of Mn^{II}. Catalase activity was observed from apoR2 with a specific activity of up to 31 ± 3 μmol O_2 produced/min/mg (units/mg). However, addition of MnCl$_2$ to samples of apoR2 had no effect on this base activity. Furthermore, upon addition of 1.46 μmol of H_2O_2, at completion 0.65 μmol of O_2 was generated, which is consistent with the known stoichiometry (2 H_2O_2:1 O_2) of catalase reactions. Since we can clearly observe by EPR spectroscopy that the added Mn^{II} is binding within R2 as a binuclear site[24] and that addition of excess H_2O_2 has no effect on the observed EPR spectra, we conclude that the manganese-substituted R2 is not catalase-active. ICP ES of apoR2 samples was performed on multiple batches of apoR2 in an attempt to identify the catalase-active metal. While metal analysis did indicate the presence of other redox active metals such as manganese (0.01/apoR2) and copper (0.02/apoR2), only residual iron content (0.1/apoR2) correlated with the catalase activity in all assayed samples. Therefore, we conclude that the previously reported catalase activity of

manganese-substituted R2 is due to an Fe species and is not associated with manganese.

Discussion

Mixed Metal Additions. A schematic representation summarizing the species and relative equilibria for sequential metal addition to apoR2 is shown in Scheme 2. For all of these steps, occupation of the second β-protomer of R2 only occurs upon reaction with oxygen. On the left side of the scheme, Mn^{II} binds within the B-site of one β-protomer of apoR2 (β_I) to produce (Mn$_B^{II}\beta_I$)(β_{II}).[24] To this species, an additional equivalent of Mn^{II} or Fe^{II} can be added to produce a binuclear cluster within a single protomer (M$_A^{II}$Mn$_B^{II}\beta_I$)(β_{II}), where M = Mn or Fe. The equilibria in both cases strongly favor full occupation of a single protomer. The (Mn$_A^{II}$Mn$_B^{II}\beta_I$)(β_{II}) cluster does not react with either H_2O_2 or O_2, whereas the mixed metal cluster (Fe$_A^{II}$-Mn$_B^{II}\beta_I$)(β_{II}) is oxidized to (Fe$_A^{III}$Mn$_B^{III}\beta_I$)(β_{II}) by H_2O_2. Thus, Fe rather than Mn is responsible for initiating the reduction of H_2O_2. Introduction of O_2 to (Fe$_A^{II}$Mn$_B^{II}\beta_I$)(β_{II}) produces R2$_{act}$ and Mn$_2^{II}$R2, according to the published stoichiometry of (1 R2$_{act}$ per 3 Fe^{II}).[24] This implies that both Mn^{II} and Fe^{II} can disassociate from the protein, and when a diferrous active site is formed, it reacts with O_2 to produce Fe$_2^{III}$(O^{2-}); Y122$\bullet$ (R2$_{act}$). The Mn^{II} can then be incorporated into either the Fe^{II} vacated sites on β_I or into β_{II} during turnover.[24] For 1 equiv of Fe^{II} added per R2 homodimer, only 0.5 equiv of the diferrous active site can potentially be produced, leaving an equal amount of apoR2 available for Mn^{II} uptake. We cannot experimentally differentiate which protomer Mn^{II} occupies.

On the right side of Scheme 2, Fe^{II} binds within the B-site of β_I to produce (Fe$_B^{II}\beta_I$)(β_{II}). Previous MCD and Mössbauer work indicates that both Mn^{II} and Fe^{II} have a greater affinity for the B-site of R2.[21,22] EPR spectroscopy indicates Fe^{II} must be bound since Mn^{II} does not bind and diferrous centers are not formed. The (Mn$_A^{II}$Fe$_B^{II}\beta_I$)(β_{II}) and (Fe$_A^{II}$Fe$_B^{II}\beta_I$)(β_{II}) complexes are not observed in significant amounts. Thus, the equilibria for both cases strongly favors single Fe^{II} incorporation, and the additional metal is observed as an aqueous species or at an adventitious site of the protein. This indicates that binding of the native Fe^{II} metal in β_I induces the same negative allosteric effect on β_{II} observed previously for Mn^{II}.[24]

The addition of H_2O_2 to the sample which is best described as (Fe$_B^{II}\beta_I$)(β_{II}) with the majority of Mn^{II} in solution results in the formation of the oxidized mixed metal cluster (Mn$_A^{III}$-Fe$_B^{III}\beta_I$)(β_{II}). We suggest that upon (equilibrium-controlled) binding of Mn^{II} to (Fe$_B^{II}\beta_I$)(β_{II}), H_2O_2 reacts irreversibly with the (Mn$_A^{II}$Fe$_B^{II}\beta_I$)(β_{II}) complex, resulting in a two-electron reduction of peroxide to water and the generation of the (Mn$_A^{III}$-Fe$_B^{III}\beta_I$)(β_{II}) complex. The trivalent metals are slow to exchange, and thus the reaction is driven to the stable oxidized species with the majority having Mn bound. Hydrogen peroxide does not react with aquaMn^{II} or (Mn$_A^{II}$Mn$_B^{II}\beta_I$)(β_{II}). Oxidation with H_2O_2 does not remove the restriction caused by the *global* conformational change, since no protein-bound Mn^{II} species are generated other than the oxidized mixed metal cluster.

The addition of H_2O_2 to aqueous solutions containing divalent metal ions can produce hydroxyl radicals ($\bullet$OH) from Fenton chemistry;[33] however, we have no evidence in support of Fenton-based chemistry. First, HO$\bullet$ would attack the protein, giving rise to protein radical species, but no such radical species

Scheme 2

OR = OH or carboxylato
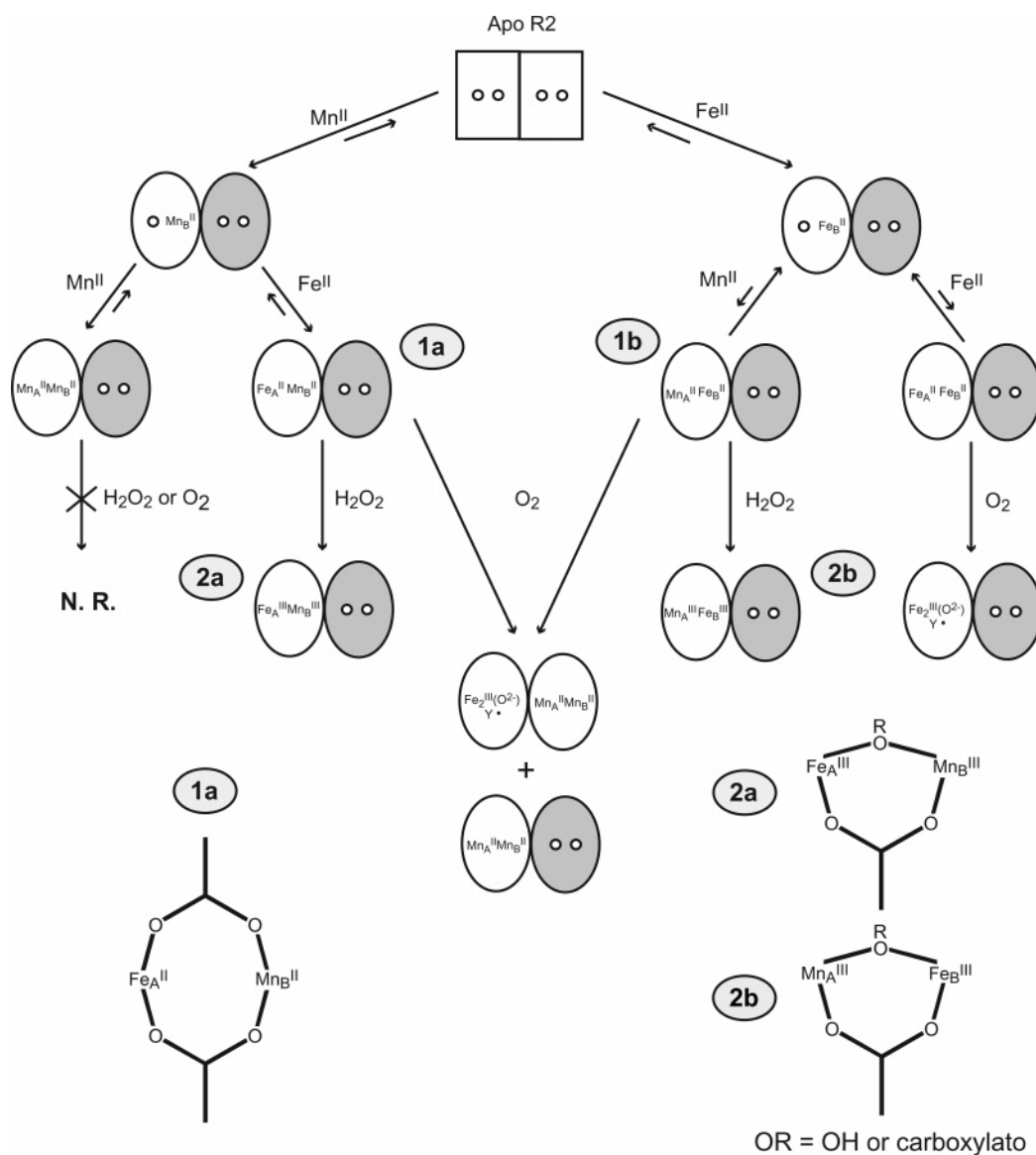
are observed in the EPR spectra. Second, the ferrous iron is bound within the B-site of R2 ($Fe_B^{II}\beta_I$)(β_{II}), and all of the added Mn^{II} is quantitatively accounted for as free aquaMn^{II}; thus, the iron is within the active site of R2 and the manganese is not. The formation of the $Mn_A^{III}Fe_B^{III}$ cluster bound *within the active site* (shown previously)[24] cannot be explained with a Fenton-type reaction. If HO• is generated outside of the protein by manganese, the Mn^{II} ion could be oxidized to Mn^{III} and disproportionate to Mn^{II} and Mn^{IV}. However, neither of these species are observed in the EPR spectra. In addition, Mn^{III} is unlikely to diffuse into the active site of R2, just as Fe^{III} does not. Third, if HO• is generated inside the protein by ($Fe_B^{II}\beta_I$) it would more likely oxidize the protein rather than diffuse out of the active site.

Similar to the left side of Scheme 2, the single turnover reaction of O_2 with ($Fe_B^{II}\beta_I$)(β_{II}) and Mn^{II} in solution produces $R2_{act}$ and $Mn_2^{II}R2$, according to the published stoichiometry of (1 $R2_{act}$ per 3 Fe^{II}).[24] Thus, exchange (scrambling) of metals occurs during reaction with O_2 to drive the formation of the stable diferric cluster. In contrast to the hydrogen peroxide addition, the single turnover reaction of O_2 with $Mn^{II}Fe^{II}$ mixed

metal clusters does not produce $Mn^{III}Fe^{III}$ clusters. However, we do observed the formation of some $Mn^{III}Fe^{III}$ clusters during multiple turnover reactions of the protein in the presence of dithionite, mediator, and O_2.[24] During these experiments, the only oxidants present are O_2 and the high oxidation states of the diiron cluster (e.g., intermediate X). Single turnover reactions of O_2 with $Mn^{II}Fe^{II}$ do not produce $Mn^{III}Fe^{III}$ clusters. Thus, the production of $Mn^{III}Fe^{III}$ clusters is due to oxidization by a high-valent diiron cluster of a different active site formed during the O_2 turnover chemistry of R2. We take this as evidence that one active site can serve as an electron source for another site in the generation of $R2_{act}$. Therefore, in part, the substoichiometric yield of Y122• per R2 could be a result of inter- and/or intraprotein electron transfer between the active sites of R2.

Fe^{II} Incorporation of apoR2. Two observations indicate that the equilibrium constant for the binding of the iron to R2 disfavors formation of dinuclear ferrous sites. First, the addition of 1 equiv of Fe^{II} to apoR2 prevents a significant amount of Mn^{II} from binding either β-strand of R2. Second, a quantitative accounting of all iron in the iron titration experiment finds relatively small amounts of dimer formation at high iron

concentrations. Thus, Fe^{II} binding within the B-site of apoR2 induces the same *global* conformational change observed for Mn^{II},[24] resulting in the restriction of metal access within β_{II}. However, unlike Mn^{II}, ferrous iron also induces a *local* change that lowers the affinity of Mn^{II} and Fe^{II} within the adjacent A-site on β_I.

On the basis of our in vitro studies of the R2 active site assembly, we suggest that prior to introduction of O$_2$, a single ferrous iron binds within the B-site of a single β-protomer of R2 (Fe$_B^{II}\beta_I$) and the A-site of this protomer is largely unoccupied. When present, O$_2$ binds to Fe$_B^{II}$, and when the (Fe$_A^{II}$-Fe$_B^{II}\beta_I$) complex forms, reaction with O$_2$ produces the oxidized (Fe$_A^{III}$Fe$_B^{III}\beta_I$) complex. Similar to the (Mn^{III}Fe$^{III}\beta_I$) complex, the trivalent iron atoms are slow to exchange and the reaction is driven to the oxidized species. If sufficient Fe is not present, scrambling of Fe will occur during the O$_2$ reaction until all iron is oxidized. The O$_2$ reaction chemistry proceeds to the formation of the (Fe$_A^{III}$Fe$_B^{III}\beta_I$) complex and Y122•, during which the remaining two ferrous iron binding sites located within the opposite β-protomer (β_{II}) become transiently available for metal.[24] These sites, upon formation of the diiron cluster, also turn over to produce Y122•.

Given the estimated abundance of available iron within the cellular labile iron pool, it is possible that these observations extends to the in vivo mechanism of assembly.[42,43] Nevertheless, R2 demonstrates a high level of interaction between the two metal binding sites within each β-protomer and between each β-protomer of the homodimer. We suggest that the allosteric effect is a *global* protein conformational change that restricts access of metal into the β_{II} protomer. Prior kinetic studies of reactions with O$_2$ have suggested a protein conformation change occurs upon preloading of Fe^{II}.[26,27] We suggest that the *local* change at the β_I active site results in a lower binding constant of the second metal for the A-site of β_I because of the occupation of the B-site with Fe^{II}. Six-coordinate high-spin Mn^{II} and Fe^{II} have effective ionic radii of 97 and 92 pm, respectively.[44] If the size of the metal ion is the dominant factor, we might expect that binding of the larger Mn^{II} ion would crowd the adjacent A-site and lower the metal affinity. Since the opposite is observed, other factors such as ligand-field stabilization for Fe^{II} must influence binding at the adjacent site.

Our observations are consistent with the previous results of Fe^{II} titrations of R2 followed by MCD spectroscopy.[21] In the MCD measurements, the protein buffer contained 50% glycerol. We have shown previously that higher glycerol concentrations remove the allosteric interaction between the protomers, allowing dinuclear metal clusters to form in both protomers during a titration.[24] In addition, higher glycerol concentrations also significantly lower the metal binding constants. The results of the titrations monitored with CD spectroscopy, which were performed in the absence of glycerol, require further explanation.

The CD titrations in the absence of glycerol also indicate the presence of two spectroscopically distinct metal sites: four-(4C) and five-coordinate (5C) binding sites. Furthermore, the 5C site was shown to have a greater binding affinity than the

4C site. The magnetic behavior of spin-coupled bimetallic sites as detected from MCD or EPR spectroscopy allows an unequivocal assignment of dinuclear metal sites in the protein, whereas the CD spectroscopic data are not quantitative and not site-specific for dinuclear metal centers. Since hexaqua Fe^{II} is not CD active, it is not possible to accurately determine the amount of either the 4C or the 5C site occupied at any point in the titration. The CD data show that the binding of the 4C site reaches a plateau near 3 equiv of added Fe^{II}.[21] Consistent with this observation, we also find (Table 2) that formation of the dinuclear site increases until 3 equiv of Fe^{II}, with less change at higher equivalents. While the EPR data cannot differentiate between the various mononuclear Fe^{II} species present, it does quantitatively account for all of the metal added to the samples. The diferrous clusters are not the predominant species formed, and thus the A-site is not saturated at 3 to 4 equiv of added Fe^{II}. Therefore, we disagree with a conclusion derived from the CD data that R2 is completely reconstituted after addition of 3.2 ferrous ions.[21] In previous work, we observed that low salt concentrations of the buffer (<25 mM) resulted in low binding of metal in the active site of R2.[24] We interpret this observation to imply the existence of adventitious metal binding sites on R2 that can compete for metal.

Properties of the Fe^{II}Mn^{II} Cluster. For the Fe^{II}Mn^{II} cluster, the high rhombicity ($E_{Fe}/D_{Fe} = 0.33$) of the Fe$_A$ site reported here for the Fe^{II}Mn^{II} cluster is consistent with the low symmetry observed in the reduced R2 crystal structure.[8,18,19] The exchange coupling for the dicarboxylato bridged Mn$_2^{II}$R2 cluster is $J = -1.8 \pm 0.3$ cm^{-1}.[24] For **1a**, we find $J = -1.3 \pm 0.4$ cm^{-1}. The number of available microstates that could take part in a super exchange pathway is lower for the Fe^{II}Mn^{II} cluster by 20/25. Thus, the decrease in the value of J for the Fe^{II}Mn^{II} cluster relative to the Mn$_2^{II}$R2 cluster by this ratio is consistent with the Fe^{II}Mn^{II}R2 cluster shown in Scheme 2, which retains two carboxylate bridges. Our J-value also agrees with previous MCD/CD studies[21] of the Mn^{II}Fe^{II} cluster ($J = -1.2 \pm 0.4$ cm^{-1}).

Properties of the Fe^{III}Mn^{III} Clusters. A comparison of the EPR signal observed for Fe^{III}Mn^{III}R2 to that of the Fe^{III}Mn^{III}*N*, *N′,N″*-trimethyl-1,4,7-triazacyclononane (TACN) complex[45] shows that the hyperfine splittings are similar. However, the exchange coupling for Fe^{III}Mn^{III}R2 is significantly lower than Fe^{III}Mn^{III}TACN, −18 cm^{-1} versus −73 cm^{-1}, respectively. This difference in the exchange coupling likely reflects differences in a bridging ligand for Fe^{III}Mn^{III}R2. The lower value of J for Fe^{III}Mn^{III}R2 is consistent with a substituted single atom bridge of the μ-hydroxo or μ-carboxylato groups shown in Scheme 2, as opposed to the μ-oxo bridge of Fe^{III}Mn^{III}TACN. At temperatures up to 50 K, the relative signal intensities of **2a** and **2b** remain unchanged, indicating that the exchange coupling, and therefore the metal bridging ligands, is independent of which metal occupies the A- and B-sites.

In the strong exchange limit, the system hyperfine splitting (A_S) and g-values (g_S) for an $S = 5/2$ Fe^{III} ion coupled to an $S = 5/2$ Mn^{III} ion are related to the intrinsic A- and g-values of the individual ions by:[46]

$$A_S = -\frac{4}{3}A_{Mn}, \qquad g_S = -\frac{4}{3}g_{Mn} + \frac{7}{3}g_{Fe} \qquad (3)$$

Assuming Fe^{III} is isotropic with $g = 2.0$,[45] the intrinsic g-values

(42) Crichton, R. *Inorganic Biochemistry of Iron metabolism. From Molecular Mechanisms to Clinical Consequences*, 2nd ed.; Wiley & Sons: New York, 2001.
(43) Thomas, F.; Serratrice, G.; Beguin, C.; Saint Aman, E.; Pierre, J. L.; Fontecave, M.; Laulhere, J. P. *J. Biol. Chem.* **1999**, *274*, 13375−13383.
(44) Huheey, J. E. *Inorganic Chemistry*, 2nd ed.; Harper & Row: New York, 1978.

for Mn^{III} (g_{Mn}) calculated from the system g-values derived from the simulation of the $Fe^{III}Mn^{III}R2$ species **2a** and **2b** are given in Table 1. Reported values for $|D_{Mn^{III}}|$ range from 1 to 5 cm^{-1}, implying that the ratio of J/D could potentially range from 4 to 18.[47−50] Therefore, the $S = 1/2$ ground doublet contains a small admixture of the $S = 3/2$ state, which contributes an uncertainty of ∼15% in the determination of the intrinsic g- and A-values. The intrinsic g-values for Mn^{III} agree with published values of other Mn^{III} complexes as listed.[47,48,51] As expected for an electronic configuration having less than a half-filled shell, the intrinsic g-values determined for the Mn^{III} site are all $< g_e$ ($g_e = 2.0023$).

Previous studies on various Mn complexes have found that the intrinsic hyperfine values for manganese are negative.[34,47,48,51−53] The observed hyperfine splitting of manganese has two contributions. The dominant contribution is the isotropic Fermi contact interaction (A_{iso}), which varies inversely with the covalency of the metal ligands at the magnetic nucleus.[34,54,55] The second contribution comprises two parts: the dipole−dipole interaction between the electron spin within a specific d-orbital and the nuclear moment (A_{dip}), and the interaction between the nuclear moment and the orbital angular momentum of the electron ($A_{orbital}$).[56] The observed deviation of g-values from g_e is small (∼0.03); thus we assume that the orbital contribution to the anisotropic component is negligible.

The A-values for Mn^{III} complexes usually display near-axial symmetry, $A_x = A_y = A_\perp$ and $A_z = A_\parallel$. The isotropic and dipolar contributions to the hyperfine tensor given in Table 1 (part II) are described by:

$$A_{iso} = \frac{(A_x + A_y + A_z)}{3}, \quad A_{dip} = A_{iso} - A_\perp = \frac{A_\parallel - A_\perp}{3} \quad (4)$$

The calculated values of A_{iso} for **2a** and **2b** are -68.0×10^{-4} cm^{-1} (-204 MHz) and -74.5×10^{-4} cm^{-1} (-223 MHz), respectively, and are similar to values reported previously for Mn^{III} ions.[34,47−53,57] The lower magnitude of A_{iso} observed for **2a** suggests increased covalency of the Mn^{III} ligands relative to **2b**. The recent high-resolution crystal structure (1.42 Å resolution)[58] of $R2_{met}$ indicates that the Fe2 site is six-coordinate while

the Fe1 site is five-coordinate. The higher coordination of Fe2 suggests that the Mn^{III} ion of **2a** is located in the Fe2 position (Fe_B).

The anisotropic contribution (A_{dip}) to the hyperfine splitting is given in Table 1 (part II). The ^5D ground term state for Mn^{III} splits into orbital triplet $^5T_2$ and doublet ^5E states. The degeneracy of the ^5E_g state is removed by Jahn−Teller distortions, resulting in either the elongation or compression of the d_{z^2} orbital. In the case of d_{z^2} elongation, the d_{z^2} orbital is occupied and a hole resides in the $d_{x^2−y^2}$ orbital.[50] The 3d^4 configuration of Mn^{III} (a hole in a half-filled shell) is analogous to the 3d^9 configuration of Cu^{II}.[49,59] Thus, neglecting orbital contributions, the ligand-field expression for A_{dip} simplifies to:[34,50,51,59,60]

$$A_{dip} = -\frac{6}{7}P' < 0 \quad \text{empty } d_{z^2} \text{ orbital} \quad (5)$$

$$A_{dip} = +\frac{6}{7}P' > 0 \quad \text{empty } d_{x^2−y^2} \text{ orbital} \quad (6)$$

in which $P' = g_e\mu_B g_N\mu_N\langle r^{-3}\rangle$. Equations 5 and 6 describe the case for an empty d_{z^2} or $d_{x^2−y^2}$ orbital. Since the sign of A_{dip} depends on the orbital configuration, the experimental data indicate which orbital is unoccupied.[53,56] In the case of **2a**, we observe $A_{dip} > 0$, indicating a ground-state electronic configuration of $(d_{xy})^1(d_{xz})^1(d_{yz})^1(d_{z^2})^1(d_{x^2−y^2})^0$, whereas the opposite is observed for **2b**, $A_{dip} < 0$, indicating a ground-state electronic configuration of $(d_{xy})^1(d_{xz})^1(d_{yz})^1(d_{x^2−y^2})^1(d_{z^2})^0$. As shown in Table 1 (part II), the observed A_{dip} for the Mn^{III} ion in the $Mn^{II}Mn^{III}$ state of *Thermus Thermophilus* manganese catalase exhibits the same sign and similar magnitude to that of **2a**, $+27.6$ and $+31.5$ MHz, respectively, indicating that both species have an empty $d_{x^2−y^2}$ orbital.[47]

Biological Significance. The most surprising finding presented here is the effect of the first equivalent of Fe^{II} on R2. Not only does binding of the first equivalent of Fe^{II} to R2 induce a negative allosteric effect on the opposite β-strand (β_{II}), but it also has a *local* effect that inhibits formation of the diferrous cluster. To our knowledge, this is the first indication that under standard buffer conditions, the diferrous active site cannot be quantitatively produced by simple titration.

We demonstrate here the ability to generate each oxidized FeMn cluster in spectroscopic purity. In all divalent metal additions, EPR spectroscopy showed no evidence of metal exchange (scrambling) over the 10 min equilibration time. Ligand exchange rates for Fe^{II} and Mn^{II} in an aqueous solution are expected to be $> 10^6$ s^{-1}. We would therefore expect scrambling of the metals if the occupation of the metal binding sites of R2 is under thermodynamic control. Since scrambling is not observed, a kinetic constraint must exist that slows the redistribution of metals within the A- and B-sites of β_I. Such a kinetic constraint has been previously invoked to explain a lag phase during the activation of R2. It was proposed that a slow conformational change occurs after binding the first equivalent of Fe^{II}.[26,27] On this basis, exchange of the B-site metal would be limited by the slower conformational step following metal binding. The work presented here strongly supports this hypothesis.

(45) Bossek, U.; Weyhermuller, T.; Wieghardt, K.; Bonvoisin, J.; Girerd, J. J. *J. Chem. Soc., Chem. Commun.* **1989**, 633−636.
(46) Bencini, A.; Gatteschi, D. *Electron Paramagnetic Resonance of Exchange Coupled Systems*; Springer-Verlag: New York, 1990.
(47) Zheng, M.; Khangulov, S. V.; Dismukes, G. C.; Barynin, V. V. *Inorg. Chem.* **1994**, *33*, 382−387.
(48) Campbell, K. A.; Yikilmaz, E.; Grant, C. V.; Gregor, W.; Miller, A.-F.; Britt, R. D. *J. Am. Chem. Soc.* **1999**, *121*, 4714−4715.
(49) Gerritsen, H. J.; Sabisky, E. S. *Phys. Rev.* **1963**, *132*, 1507−1512.
(50) Campbell, K. A.; Force, D. A.; Nixon, P. J.; Dole, F.; Diner, B. A.; Britt, R. D. *J. Am. Chem. Soc.* **2000**, *122*, 3754−3761.
(51) Peloquin, J. M.; Campbell, K. A.; Randall, D. W.; Evanchik, M. A.; Pecoraro, V. L.; Armstrong, W. H.; Britt, R. D. *J. Am. Chem. Soc.* **2000**, *122*, 10926−10942.
(52) Reed, G. H.; Markham, G. D. *Biol. Magn. Reson.* **1984**, *6*, 73−142.
(53) Bencini, A.; Gatteschi, D. *Inorg. Electron. Struct. Spectrosc.* **1999**, *1*, 93−159.
(54) McGarvey, B. R. *J. Phys. Chem.* **1967**, *71*, 51−67.
(55) Penfield, K. W.; Gewirth, A. A.; Solomon, E. I. *J. Am. Chem. Soc.* **1985**, *107*, 4519−29.
(56) Palmer, G. In *Physical Methods in Bioinorganic Chemistry: Spectroscopy and Magnetism*; Que, L., Jr., Ed.; University Science Books: Sausalito, CA, 2000; pp 121−185.
(57) Krzystek, J.; Telser, J.; Pardi, L. A.; Goldberg, D. P.; Hoffman, B. M.; Brunel, L.-C. *Inorg. Chem.* **1999**, *38*, 6121−6129.
(58) Hogbom, M.; Galander, M.; Andersson, M.; Kolberg, M.; Hofbauer, W.; Lassmann, G.; Nordlund, P.; Lendzian, F. *Proc. Natl. Acad. Sci. U.S.A.* **2003**, *100*, 3209−3214.

(59) Griffith, J. S. *The Theory of Transition-Metal Ions*; Cambridge University Press: London, 1961.
(60) Pilbrow, J. R. *Transition Ion Electromagnetic Resonance*; Oxford University Press: New York, 1990.

Given the difficulty in producing significant levels of $Fe_2^{II}R2$ sites by simple titration in vitro, it is possible that the in vivo mechanism for active site assembly does not occur by simple sequential occupation of iron into the active site. Our studies demonstrate a communication between the β-strands of R2 and a possible sequence of events that occur within the protein upon activation, both of which testify to the overall complexity of the protein and, subsequently, RNR.

Finally, this work demonstrates that incorporation of Mn^{II} into R2 does not impart any catalase activity above that of the baseline apoR2 activity and should therefore not be considered a functional model for dimanganese catalases.